

Tailoring Solution Accuracy for Fast Whole-body Model Predictive Control of Legged Robots

Charles Khazoom¹, Seungwoo Hong¹, Matthew Chignoli¹, Elijah Stanger-Jones¹ and Sangbae Kim¹

Abstract—Thanks to recent advancements in accelerating non-linear model predictive control (NMPC), it is now feasible to deploy whole-body NMPC at real-time rates for humanoid robots. However, enforcing inequality constraints in real time for such high-dimensional systems remains challenging due to the need for additional iterations. This paper presents an implementation of whole-body NMPC for legged robots that provides low-accuracy solutions to NMPC with general equality and inequality constraints. Instead of aiming for highly accurate optimal solutions, we leverage the alternating direction method of multipliers to rapidly provide low-accuracy solutions to quadratic programming subproblems. Our extensive simulation results indicate that real robots often cannot benefit from highly accurate solutions due to dynamics discretization errors, inertial modeling errors and delays. We incorporate control barrier functions (CBFs) at the initial timestep of the NMPC for the self-collision constraints, resulting in up to a 26-fold reduction in the number of self-collisions without adding computational burden. The controller is reliably deployed on hardware at 90 Hz for a problem involving 32 timesteps, 2004 variables, and 3768 constraints. The NMPC delivers sufficiently accurate solutions, enabling the MIT Humanoid to plan complex crossed-leg and arm motions that enhance stability when walking and recovering from significant disturbances.

I. INTRODUCTION

Legged robots have great potential for applications requiring animal-like mobility, but their high dimensionality, non-linearity, and underactuation make them difficult to control.

Reinforcement learning (RL) policies showed promise in addressing these challenges, partly because they are trained in mature high-fidelity simulators with whole-body dynamics and kinematics. However, RL requires vast amounts of data.

Non-linear model predictive control (NMPC) is another powerful tool for providing closed-loop stability to constrained non-linear systems. Unlike RL, NMPC uses a model to rapidly design new behaviors via online optimization. Yet, achieving real-time rates for high-dimensional systems like legged robots is challenging, especially when aiming for highly accurate optimal solutions with inequality constraints. However, real robotic systems may not always benefit from high-accuracy solutions due to modeling errors and delays.

We present an implementation of whole-body NMPC with inequality constraints. Using a suitable solver, we tailor solution accuracy to the computational budget and improve self-collision avoidance using control barrier functions (CBFs) at the first timestep of the NMPC. We demonstrate our

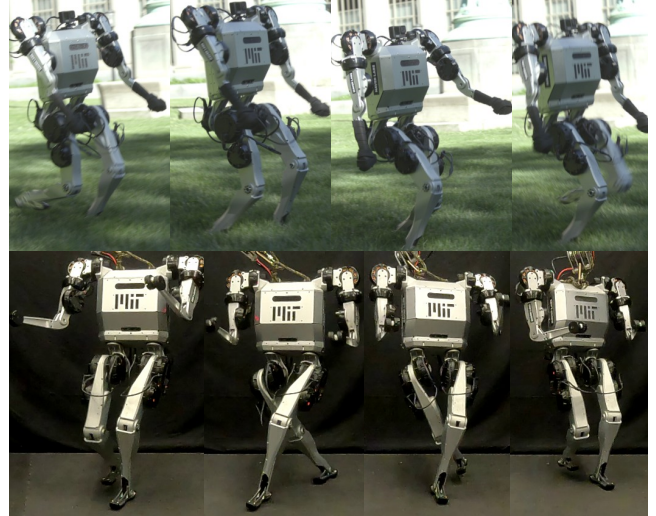


Fig. 1: Hardware demonstration of the whole-body NMPC on the MIT Humanoid. Top row: walking with emergent arm swing. Bottom row: leg crossing with dynamic self-collision avoidance with right leg fully extended during abrupt halting during lateral walking.

approach through extensive simulation and hardware walking experiments on the MIT Humanoid (Fig. 1).

A. Multilayered Controller Architectures for Legged Robots

To reduce the computational burden of NMPC for legged robots, the problem is usually broken down into smaller multilayered optimizations that are easier to solve. A common architecture uses MPC with reduced-order models, whose outputs are tracked by an inverse dynamics whole-body controller (WBC) [1], [2]. These simple models enable fast computation, but cannot account for all degrees of freedom and constraints like joint position limits, torque limits and self-collisions, which require holistic whole-body reasoning.

This issue can be partly addressed by reactive WBCs which project desired accelerations on the constraints of a whole-body model. The constraints are typically limited to ones at the acceleration level like friction cone or torque constraints, but non-linear constraints on the robot’s configuration can be incorporated via control barrier functions (CBFs) [3], [4]. For instance, exponential CBFs [5] were previously incorporated in a WBC for self-collision avoidance. These reactive WBCs benefit from exact linearization at the current state, resulting in small quadratic programs solvable at high frequency by off-the-shelf solvers. However, they are myopic to the future. Additionally, multilayered architectures can produce conflicts between the reduced-order MPC and the WBC since they use different models, horizons and constraints. Ideally,

This work was supported by Naver Labs, NSERC and FRQNT.

¹Department of Mechanical Engineering Department, Massachusetts Institute of Technology, 77 Massachusetts Ave, Cambridge, MA, United States
ckhaz@mit.edu, sangbae@mit.edu

we would need a single planner that incorporates all the robot’s degrees of freedom and constraints and provides real-time solutions for long-horizon tasks. However, incorporating whole-body dynamics, kinematics and arbitrary constraints within a single NMPC controller is still computationally challenging for high-dimensional systems.

B. Solution Methods for Real-Time NMPC of Legged Robots

Roboticians have developed various strategies to address the computational burden of whole-body NMPC. The most common solution methods for NMPC include sequential quadratic programming (SQP) [6] and differential dynamic programming (DDP) [7], both of which solve a local convex subproblem at each iteration. Solving NMPC to optimality can be prohibitively slow; therefore, only one or a few iterations are typically performed online at each control instant [8]. Furthermore, specialized matrix factorization methods that exploit the temporal structure of the problem (e.g., Riccati recursion), specialized algorithms for analytical derivatives [9]–[11] and parallelization [10], [12] enabled real-time NMPC on hardware for quadrupeds [4], [13]–[15] and humanoids [16], [17].

Despite these advancements, inequality constraints are still hard to enforce in real time for high-dimensional systems since they unavoidably require additional expensive inner iterations to solve the local subproblems. For instance, interior point solvers [18]–[20] require multiple matrix factorizations and active set methods scale poorly with the number of inequalities [6], [21]. Augmented Lagrangian approaches have increased in popularity for handling constraints for QP [20], [22] and trajectory optimization solvers [23], [24]. Yet, even the most advanced implementations of whole-body NMPC for legged robots relax inequality constraints like friction cone, joint limits and self-collisions in the cost function using penalty methods [4], [23], [25]. This technique increases the coupling between cost minimization and constraint satisfaction [26], leading to time-consuming and task-specific tuning. Sleiman *et al.* [26] proposed an online scheme based on the method of multipliers to handle inequality constraints but can only afford a single update of the decision variables and Lagrange multipliers per control instant [14], [26].

Another augmented Lagrangian technique for solving QP subproblems is the alternating direction method of multipliers (ADMM) [27]. ADMM is a general framework that splits optimization problems into smaller subproblems that are easier to solve and has gained popularity in robotics [28]–[31]. In particular, the operator splitting QP solver OSQP leverages ADMM to handle linear equality and inequality constraints while only requiring a single sparse matrix factorization followed by multiple cheap iterations [32]. Yet, there is currently no demonstration of its applicability for solving the QP subproblems arising in whole-body NMPC of legged robots in real time, even though some SQP implementations using OSQP exist [33], [34] and have been deployed on lower-dimensional robot manipulators [35]. While ADMM may need many iterations to provide high-accuracy solutions,

it can rapidly converge to low-accuracy solutions and be warm-started, making it a practical option for solving very complex NMPC problems in real time.

C. Contributions

The main contributions of this paper are threefold. First, we present a whole-body NMPC formulation that leverages ADMM to solve the inner QP subproblem of an SQP method with inequality constraints in real time. Through extensive simulation, we demonstrate the advantages of rapid, low-accuracy solutions obtained from ADMM by benchmarking the impact of solution accuracy on closed-loop performance in the presence of unavoidable inertial modeling errors, dynamics discretization errors, and computation delay.

Second, we enhance the closed-loop feasibility of low-accuracy solutions by incorporating CBF constraints at the first timestep of the NMPC. These constraints are easier to satisfy due to exact linearization at the measured state, making them independent of the initial guess. This approach enables stricter self-collision avoidance within the NMPC with minimal added complexity while avoiding conflicts that arise in multilayered controllers.

Lastly, we validate our approach through comprehensive hardware experiments on the MIT Humanoid. These experiments demonstrate the emergence of coordinated whole-body movements, including stabilizing arm and crossed-leg motions. The robot reliably respects joint limits, self-collisions and contact constraints while walking and recovering from significant external disturbances.

The paper is organized as follows. Section II presents the NMPC formulation and the SQP method to solve it. Section III presents the simulation analyses. Section IV presents the hardware demonstration on the MIT Humanoid.

II. CONTROLLER DESIGN

This section presents background on NMPC, details our proposed NMPC formulation, and the solution strategy for solving it in real time.

A. Background on Non-linear MPC

NMPC closes the loop by continuously solving the non-linear trajectory optimization problem (1) with horizon $N \in \mathbb{N}$ and applying the first control input \mathbf{u}_0 as the state of the robot evolves:

$$\min_{\mathcal{X}} \sum_{k=0}^{N-1} l(\mathbf{x}_k, \mathbf{u}_k, \boldsymbol{\theta}) + l_N(\mathbf{x}_N, \boldsymbol{\theta}) \quad (1a)$$

subject to

$$\mathbf{x}_0 = \hat{\mathbf{x}} \quad (1b)$$

$$\mathbf{x}_{k+1} = \mathbf{f}(\mathbf{x}_k, \mathbf{u}_k, \boldsymbol{\theta}) \quad \forall k \in \{0, \dots, N-1\} \quad (1c)$$

$$\mathbf{g}(\mathbf{x}_k, \mathbf{u}_k, \boldsymbol{\theta}) \leq \mathbf{0} \quad \forall k \in \{0, \dots, N-1\} \quad (1d)$$

$$\mathbf{g}_N(\mathbf{x}_N, \boldsymbol{\theta}) \leq \mathbf{0}, \quad (1e)$$

where \mathcal{X} is the set of decision variables composed of the states \mathbf{x}_k and control inputs \mathbf{u}_k at stage $k \in \{0, \dots, N\}$, $\hat{\mathbf{x}}$ is the measured state, $\boldsymbol{\theta}$ is a parameter vector, $l(\cdot)$ is the

running cost, $l_N(\cdot)$ is the terminal cost, $\mathbf{f}(\cdot)$ is the discrete-time dynamics, $\mathbf{g}(\cdot)$ and $\mathbf{g}_N(\cdot)$ are the path equality and inequality constraints.

B. Whole-body Non-Linear MPC Formulation

1) *Decision Variables*: The whole-body NMPC solves for the set of decision variables \mathcal{X} :

$$\mathcal{X} = \{\{\mathbf{q}_k, \mathbf{v}_k\}_{k=0}^N, \{\boldsymbol{\tau}_k, \mathbf{F}_{c,k}\}_{k=0}^{N-1}\}. \quad (2)$$

For a robot with n_j actuated joints, \mathcal{X} includes the robot's configuration $\mathbf{q} \in \mathbb{R}^{n_j+6}$, generalized velocity $\mathbf{v} \in \mathbb{R}^{n_j+6}$, the joint torques $\boldsymbol{\tau} \in \mathbb{R}^{n_j}$ and the contact forces $\mathbf{F}_c \in \mathbb{R}^3$ for each contact point $c \in \mathcal{C}$. The configuration \mathbf{q} is composed of the floating base position $\mathbf{p} \in \mathbb{R}^3$, Euler angle orientation $\boldsymbol{\Theta} \in \mathbb{R}^3$, and joint position $\mathbf{q}_j \in \mathbb{R}^{n_j}$. The velocity \mathbf{v} includes the spatial velocity of the floating base $\mathbf{v}_b \in \mathbb{R}^6$ and the joint velocity $\dot{\mathbf{q}}_j \in \mathbb{R}^{n_j}$.

2) *Cost Function*: We use a simple quadratic cost function that penalizes the deviation from constant velocity and torso height commands along the NMPC horizon. We use simple regularization for all other decision variables. The difference between the decision variable $\boldsymbol{\tau}_0$ and its value from the previous solution is penalized to eliminate vibrations on hardware. The cost function has a least-squares form. Therefore, we approximate the Hessian of the Lagrangian with the Gauss-Newton Hessian to reduce solve time [8].

3) *Dynamics Constraints*: The discrete-time dynamics are described as:

$$\mathbf{q}_{k+1} = \mathbf{q}_k + \frac{1}{2}\mathbf{B}(\boldsymbol{\Theta}_k)(\mathbf{v}_{k+1} + \mathbf{v}_k)dt_k, \quad (3)$$

where dt_k is the dynamics discretization timestep and $\mathbf{B}(\boldsymbol{\Theta})$ maps \mathbf{v} to $\dot{\mathbf{q}}$.

The trajectory is constrained by the inverse dynamics $\mathbf{f}_{\text{RNEA}}(\cdot)$, efficiently computed with the recursive Newton-Euler algorithm (RNEA):

$$\begin{bmatrix} \mathbf{0}_{6 \times 1} \\ \boldsymbol{\tau}_k \end{bmatrix} = \mathbf{f}_{\text{RNEA}}(\mathbf{q}_k, \mathbf{v}_k, \dot{\mathbf{v}}_k) - \sum_{c \in \mathcal{C}} \mathbf{J}_{c,k}^\top \mathbf{F}_{c,k}, \quad (4)$$

where $\mathbf{J}_c \in \mathbb{R}^{3 \times (n_j+6)}$ is the Jacobian of contact point c . The wrench on the floating base is zeroed, and $\boldsymbol{\tau}_k$ corresponds to the last n_j rows in (4). The acceleration $\dot{\mathbf{v}}_k$ is computed from finite differences:

$$\dot{\mathbf{v}}_k = \frac{\mathbf{v}_{k+1} - \mathbf{v}_k}{dt_k}. \quad (5)$$

4) *Contact and Swing Constraints*: The NMPC takes as input a contact sequence $\theta_{c,k} \in \{0, 1\}$ for each contact point c and stage k , where $\theta_{c,k} = 1$ in contact and $\theta_{c,k} = 0$ in swing. Contact forces are constrained to $\mathbf{0}_{3 \times 1}$ in swing and to the friction cone in stance:

$$(1 - \theta_{c,k})\mathbf{F}_{c,k} = \mathbf{0}_{3 \times 1} \quad (6)$$

$$\theta_{c,k} \mu F_{c,z,k} \geq \theta_{c,k} \sqrt{F_{c,x,k}^2 + F_{c,y,k}^2}, \quad (7)$$

where $F_{c,x,k}$ and $F_{c,y,k}$ are the world-frame tangential forces in the forward and lateral directions. The multiplication by $(1 - \theta_{c,k})$ and $\theta_{c,k}$ respectively deactivates the constraints in

stance and swing without removing them from the problem at runtime. This keeps the sparsity structure of the QP subproblems fixed, which facilitates warmstart and avoids repeating expensive symbolic factorizations.

The heights of the contact points $f_{c,z}(\mathbf{q}_k)$ are constrained to follow a reference height $z_{c,k}$:

$$f_{c,z}(\mathbf{q}_k) = z_{c,k}. \quad (8)$$

Similarly, the tangential velocity of the contact points is zeroed in stance:

$$\theta_{c,k} \mathbf{J}_{c,xy,k} \dot{\mathbf{q}}_k = \mathbf{0}_{2 \times 1}, \quad (9)$$

where $\mathbf{J}_{c,xy,k}$ maps $\dot{\mathbf{q}}_k$ to the velocity tangent to the ground. We use the adaptive segmentation algorithm detailed in [36] to segment each $\theta_{c,k}$ and dt_k to match the specified gait.

5) *Box and Kinematic Inequality Constraints*: Simple box constraints are applied to \mathbf{q}_j , $\dot{\mathbf{q}}_j$, and $\boldsymbol{\tau}$ to respect joint position, velocity and torque limits. To avoid self-collisions, non-linear kinematic inequality constraints are enforced:

$$\mathbf{h}(\mathbf{q}_k) \geq \mathbf{0}. \quad (10)$$

Equation (10) can be simple distance constraints that prevent the right foot from crossing a virtual plane attached to the left foot (Fig. 2a), or the signed-distance functions between spheres (Fig. 2b). We used the former in Section III to simplify analysis and the latter on the real robot to plan more complex motions with crossed legs.

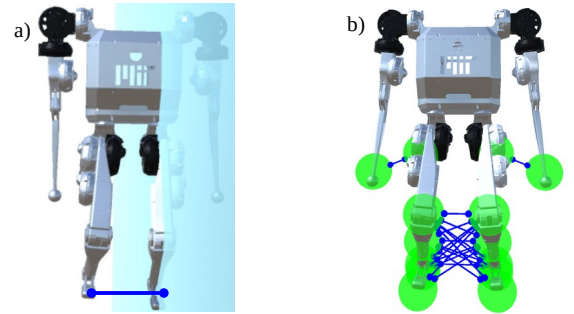


Fig. 2: Two self-collision models. a) the simple collision model constrains the right foot to a minimum distance from a plane attached to the left foot. b) the complex collision model composed of 19 pairs of spheres. Each blue line corresponds to a distance constraint between a pair of spheres.

6) *Control Barrier Functions*: The self-collision constraints (10) are highly non-linear and challenging to satisfy with less than one-centimeter accuracy when the robot experiences significant disturbances, especially in the real-time setting where a single SQP iteration is performed at each control instant. Another option to strictly enforce (10) is to use exponential CBFs [3], [5], [37], which constrain $\dot{\mathbf{v}}$ to ensure future satisfaction of (10). The CBF constraint is

$$\mathbf{J}_h \dot{\mathbf{v}} + \dot{\mathbf{J}}_h \dot{\mathbf{q}} + (\alpha_1 + \alpha_2) \mathbf{J}_h \dot{\mathbf{q}} + (\alpha_1 \alpha_2) \mathbf{h}(\mathbf{q}) \geq \mathbf{0}, \quad (11)$$

where $\mathbf{J}_h(\mathbf{q})$ is the Jacobian of $\mathbf{h}(\mathbf{q})$ with respect to \mathbf{q} , and α_1, α_2 are scalars that bound the time-response of $\mathbf{h}(\mathbf{q})$. This constraint has proven effective for reactive self-collision avoidance in humanoid robots [5] and relates to the CBF-QP safety filter [38].

When applied at the first timestep, (11) is evaluated at the measured state, making it linear and independent of the initial guess. These properties make it less susceptible to solver inaccuracies arising from performing a single SQP iteration and early termination of the ADMM QP solver. Thus, we apply (11) at the first timestep and (10) at the remaining timesteps. The former is more conservative but easier to solve, while the latter allows for planning more complex motions.

C. Solution Method

The NMPC formulation is expressed in the form of the general non-linear program (12)

$$\begin{aligned} & \min_{\mathbf{z}} C(\mathbf{z}, \boldsymbol{\theta}) \\ \text{s.t. } & \mathbf{L}(\boldsymbol{\theta}) \leq \mathbf{G}(\mathbf{z}, \boldsymbol{\theta}) \leq \mathbf{U}(\boldsymbol{\theta}), \end{aligned} \quad (12)$$

where \mathbf{z} is the decision variable vector, $\boldsymbol{\theta}$ is the parameter vector, $C(\cdot)$ is the cost function, $\mathbf{G}(\cdot)$ is the vector of constraints with lower and upper bounds $\mathbf{L}(\cdot)$ and $\mathbf{U}(\cdot)$.

One SQP step with the Gauss-Newton Hessian approximation consists in solving the following local QP subproblem at each iteration i :

$$\begin{aligned} & \min_{\mathbf{d}_i} \frac{1}{2} \mathbf{d}_i^T \nabla_{\mathbf{z}}^2 C(\mathbf{z}_i, \boldsymbol{\theta}) \mathbf{d}_i + \nabla_{\mathbf{z}} C(\mathbf{z}_i, \boldsymbol{\theta})^T \mathbf{d}_i \\ \text{s.t. } & \mathbf{L}(\boldsymbol{\theta}) \leq \mathbf{G}(\mathbf{z}_i, \boldsymbol{\theta}) + \nabla_{\mathbf{z}} \mathbf{G}(\mathbf{z}_i, \boldsymbol{\theta}) \mathbf{d}_i \leq \mathbf{U}(\boldsymbol{\theta}), \end{aligned} \quad (13)$$

where \mathbf{d}_i is the step direction, $\nabla_{\mathbf{z}} C^T$ is the gradient of $C(\cdot)$ with respect to \mathbf{z} , $\nabla_{\mathbf{z}} \mathbf{G}$ is the Jacobian of $\mathbf{G}(\cdot)$, and $\nabla_{\mathbf{z}}^2 C$ is the Hessian of the quadratic cost $C(\cdot)$ and corresponds to the Gauss-Newton Hessian. The solution is updated as follows:

$$\mathbf{z}_{i+1} = \mathbf{z}_i + \beta_i \mathbf{d}_i, \quad (14)$$

where β_i is obtained from the linesearch algorithm from [4].

Solving (13) is the most computationally expensive step, especially when inequality constraints are present. In this work, we solve (13) using the ADMM algorithm from the QP solver OSQP [32], which provides low-accuracy solutions within a few cheap iterations and can easily be restarted. This allows to tailor the solution accuracy to the computational budget by running a small but fixed number of iterations at high rates. The feasibility of the self-collision avoidance constraint (10) is enhanced by applying the CBF constraint (11) at the first timestep. Overall, our approach allows to enforce equality and inequality constraints in real time with sufficient accuracy for hardware deployment.

D. Implementation Details

The controller architecture for the MIT Humanoid is composed of the NMPC, whose trajectories are interpolated at 1 kHz and fed in the motor-level PD controller running at 20 kHz.

1) *The MIT Humanoid*: The MIT Humanoid [39] stands 1.04 m tall and weighs 24 kg. It has 24 degrees of freedom, and each leg and arm have five and four actuated joints, respectively ($n_j = 18$). The feet don't have ankle roll, making dynamic locomotion necessary since there is no support polygon when in single-leg stance. A parallel belt

transmission actuates the knee and ankle joints. This couples the knee and ankle but allows the motors to be closer to the torso. All computations run on an onboard UP Xtreme i12 computer with a Core i7-1270PE CPU.

2) *NMPC Implementation for the MIT Humanoid*: The robot's spinning rotors can contribute significantly to its dynamics and are therefore included in the dynamics model. The particularly challenging effects of the coupled knee and ankle rotors are handled via the constraint embedding-based algorithms [40] implemented in [41]. The NMPC formulation uses two contact points per foot, i.e. $\mathcal{C} = \{\text{Right Heel, Right Toe, Left Heel, Left Toe}\}$. The gait sequence is specified individually for each contact point to enable smoother heel-to-toe and toe-to-heel gaits. Because the MIT Humanoid has been designed for high-power jumping tasks [39], walking tasks are not torque-limited. Thus, the joint torque box constraint and the last n_j rows of constraint (4) are only applied for the first two timesteps to reduce the computation time. The constraints and derivatives required by (13) are computed using CasADi's automatic differentiation and codegeneration tools [33].

We run a single SQP iteration at every control instant, and the QP solver runs a fixed number of iterations. This allows to update solutions at deterministic rates and facilitates prediction delay compensation, which is performed by linearly interpolating the solved trajectory forward in time.

The whole-body NMPC is implemented in C++ and runs at 90-200 Hz on the robot's computer, depending on the formulation used. All NMPC computations run on a single thread, as opposed to most other whole-body NMPC implementations relying on multithreading to reduce computation time [4], [10], [12], [16], [17].

3) *Low-level Control*: The joint positions, velocities and torques solved by the NMPC are interpolated at 1 kHz. The resulting feedforward torque $\boldsymbol{\tau}_{\text{ff}}$, position and velocity setpoints \mathbf{q}_{des} , $\dot{\mathbf{q}}_{\text{des}}$ are fed in the motor-level controller, where the commanded motor torque $\boldsymbol{\tau}_{\text{m}}$ is computed by the following PD control law at 20 kHz:

$$\boldsymbol{\tau}_{\text{m}} = \boldsymbol{\tau}_{\text{ff}} + \mathbf{K}_{\text{p}}(\mathbf{q}_{\text{des}} - \mathbf{q}) + \mathbf{K}_{\text{d}}(\dot{\mathbf{q}}_{\text{des}} - \dot{\mathbf{q}}). \quad (15)$$

The matrices \mathbf{K}_{p} and \mathbf{K}_{d} are diagonal matrices with elements set to 50 N·m/rad and 2 N·m·s/rad, respectively.

III. SIMULATION EXPERIMENTS

The goal of the simulation experiments is to assess the effect of the solution accuracy of the QP subproblem (13) on closed-loop performance considering three unavoidable sources of error: inertial modeling errors, dynamics discretization errors, and computation delay. Additionally, we evaluate the impact of CBFs on self-collision avoidance.

A. Experimental Setup

The NMPC controller employs an approximate contact model with coarse dynamics integration timesteps as detailed in Section II-B, but is evaluated in a custom high-fidelity simulator. This simulator strictly enforces contact complementarity constraints, friction cone, and actuator torque-speed limits with a fine simulation timestep of 0.5 ms.

To thoroughly evaluate a controller’s closed-loop performance, we conduct large-scale simulations comprising 500 individual runs, each lasting 6 seconds. During each simulation, the robot is initialized in the same standing pose. It starts walking while subjected to a constant velocity command $\mathbf{v}_{\text{cmd}} = [v_{x,\text{cmd}}, v_{y,\text{cmd}}, \omega_{z,\text{cmd}}] \in [-3, 3] \text{ m/s} \times [0, 2] \text{ m/s} \times [0, 5] \text{ rad/s}$, where $v_{x,\text{cmd}}$, $v_{y,\text{cmd}}$, and $\omega_{z,\text{cmd}}$ are the forward, lateral, and turning velocity commands, respectively. A simulation is deemed successful if the robot avoids falling and satisfies the simple self-collision constraints (Fig. 2a) throughout the entire duration.

We repeat all 500 simulations for different levels of solution accuracy, inertial modeling errors and dynamics discretization errors. Solution accuracy is progressively improved by varying the number of ADMM iterations at termination from 20 to 200 iterations. The inertial modeling errors are introduced in the simulated robot by randomly varying the mass, center of mass location and moments of inertia of each link by $\pm 10, 20, 30$ and 40% . Dynamics discretization errors are introduced in the NMPC by increasing the integration timestep dt from 20 ms to 50 ms while keeping a constant time horizon of 0.8 s. A larger dt reduces the number of decision variables and solve times at the expense of reduced model fidelity. The simulations are performed in parallel using the MIT Supercloud High Performance Computing cluster [42]. Finally, we add the CBFs and compare their effect for $dt = 25$ ms.

For each controller tested, we analyse the number of successful simulations, normalized by the maximum number of successes obtained by the most successful controller (i.e. with $dt = 20$ ms at 150 ADMM iterations and without inertial modeling error).

B. Effect of Inertial Modeling Errors

Fig. 3a shows the number of successful simulations against the number of ADMM iterations for increasing inertial modeling errors. The number of successes increases with the number of ADMM iterations. However, inertial modeling errors render higher-accuracy solutions less effective. Fig. 3b shows the difference between the number of successes at 20 ADMM iterations and the maximum number of successes from Fig. 3a for each level of inertial model randomization. This assesses the potential success improvement obtainable by increasing solution accuracy when computation delay is neglected. The potential for success improvement reduces as modeling errors increase, indicating that the real MIT Humanoid may not benefit significantly from higher solution accuracy. These effects are expected to be more pronounced on hardware. For example, our simulator does not account for foot rolling contact, backlash, transmission compliance, torque-dependent friction [43], sensor noise, or low-level current control.

C. Effect of Dynamics Discretization Error

We draw similar observations as in Section III-B for the effects of dynamics discretization errors. Fig. 4a shows the normalized number of successful simulations against the

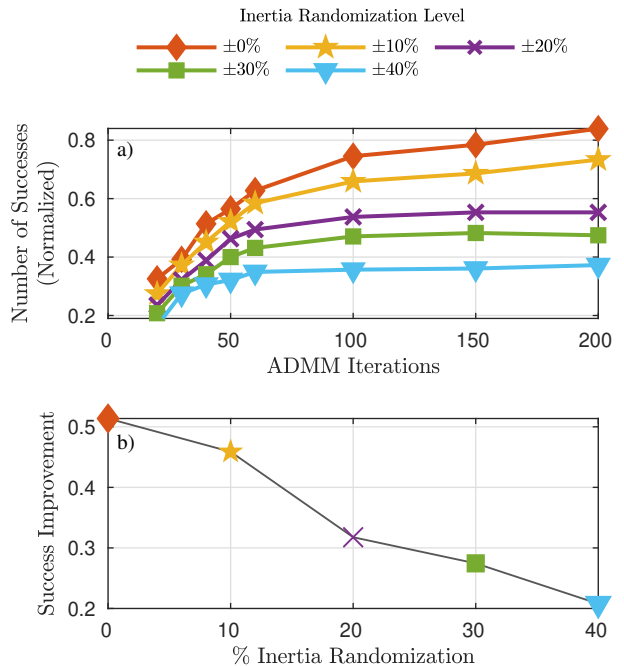


Fig. 3: a) Normalized number of successes for increasing ADMM iterations and inertial modeling errors without CBFs and computation delay. b) Potential improvement between 20 ADMM iterations and maximum success as a function of the inertia randomization level of the simulated model.

number of ADMM iterations. Between 20 to 40 iterations, the controllers with $dt \in \{20, 25, 30\}$ ms perform identically, and it takes many more iterations for $dt = 20$ ms to outperform the coarser timesteps.

The formulations with larger dt benefit less from increasing solution accuracy. As in Fig. 3b, Fig. 4b shows the potential success improvement for each discretization timestep. The potential success improvement decreases for larger timesteps, indicating that models with larger discretization errors, typically used for real-time NMPC, may not benefit as much from increased solution accuracy when used in a high-fidelity simulator and on hardware. For instance, the least accurate controller that is still stable on hardware ($dt = 50$ ms) does not benefit from running more than 20 ADMM iterations. Even though it has the lowest number of successes, it has still been successfully deployed on hardware for a walking speed of up to 0.8 m/s.

D. Effect of Computation Delay

Even though controllers with accurate models benefit the most from accurate solutions, the longer computation times offset these benefits. Fig. 5 illustrates the impact of delay on the number of successes for timesteps of $dt \in \{20, 25\}$ ms. The formulation with $dt = 20$ ms is too slow for real-time use due to its longer horizon ($N = 54$). The delay renders higher accuracy solutions ineffective despite using prediction delay compensation. Conversely, for $dt = 25$ ms and above, the computation time is sufficiently short to benefit from increased ADMM iterations. Specifically, for $dt = 25$ ms, the number of successes increases from 20 to 30 ADMM iterations but declines beyond that point.

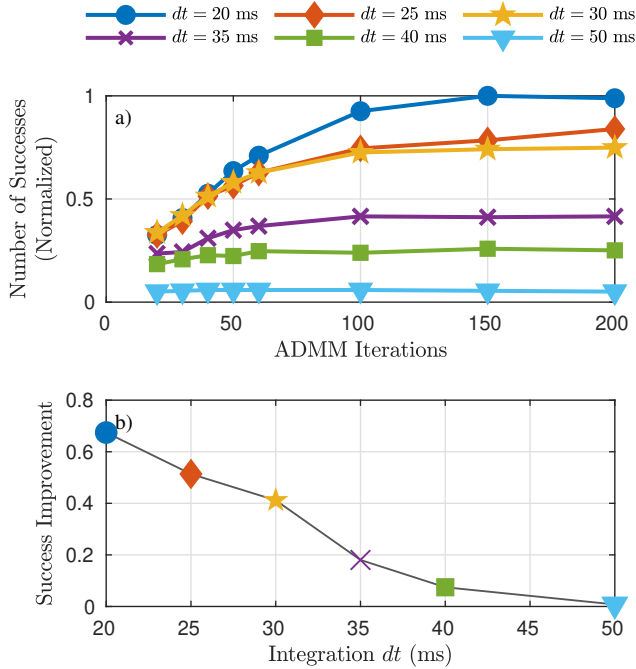


Fig. 4: a) Normalized number of successes for increasing ADMM iterations and integration timestep without CBFs and computation delay. b) Potential improvement between 20 ADMM iterations and maximum success as a function of the discretization timestep for a fixed time horizon of 0.8 s.

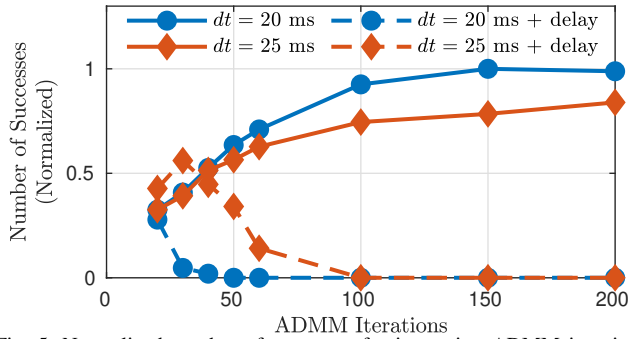


Fig. 5: Normalized number of successes for increasing ADMM iterations with and without computation delay for $dt \in \{20, 25\}$ ms.

E. Effect of Control Barrier Functions

Fig. 6 illustrates the number of successes (a), falls (b), and self-collisions (c) for $dt = 25$ ms, with and without CBFs. Without CBFs, the solutions from ADMM yield a small number of falls within 12% of the minimum number of falls at 20 iterations, but the number of collisions reduces by 4.3 times from 20 to 200 iterations.

The CBF constraints at the first timestep are independent of the initial guess and, therefore, easier to satisfy. As a result, they almost eliminate the self-collisions, regardless of the number of ADMM iterations. The number of falls increases by up to 10% since CBFs prevent infeasible motions such as penetrating legs. Overall, the number of successes doubles at 20 ADMM iterations and matches the success level obtained at 100 iterations without CBFs.

We further illustrate the effect of CBFs in a lateral push experiment, where the robot recovers from a leftward force applied to the torso while the left leg is in stance and the right leg is in swing. This scenario is challenging because

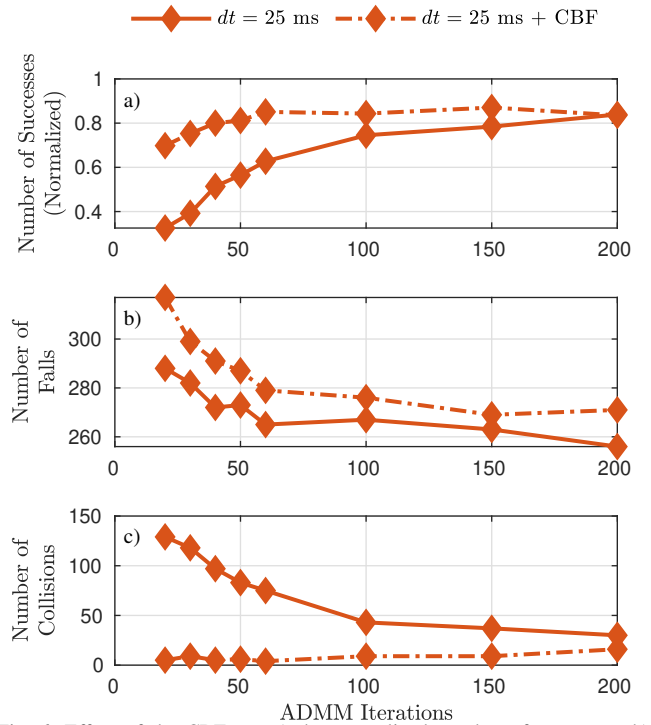


Fig. 6: Effect of the CBFs on a) the normalized number of successes, b) the number of falls and c) the number of self-collisions for $dt = 25$ ms.

the right swing leg must step as close as possible to the left stance leg without colliding to avoid falling. Fig. 7 shows the distance constraint between the feet for different strategies: ADMM without CBFs, ADMM with CBFs, and the relaxed-barrier penalty method from [4] for a disturbance applied at 0.35 s. For ADMM without CBFs, the distance constraint is violated by 3.7 cm at 0.45 s. However, sufficient SQP iterations allow the robot to recover with feasible narrow stepping that minimizes lateral torso velocity after 2 s. The penalty method achieves lower constraint violation (1.6 cm), but couples cost minimization and constraint satisfaction, leading to suboptimal wider steps after 1.5 s. Our approach, combining which combines ADMM and CBFs, maintains strict constraint satisfaction without altering the optimal narrow stepping behavior after recovering recovery.

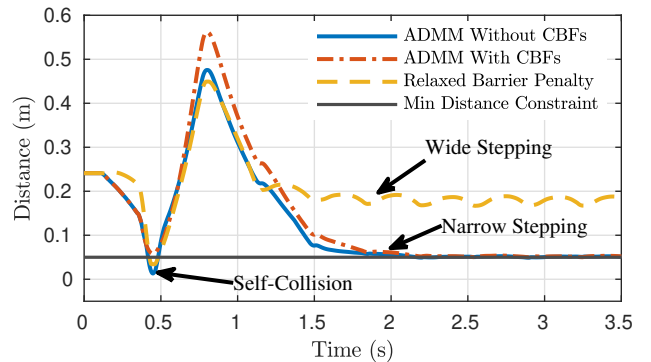


Fig. 7: Distance constraint between the feet for a lateral push recovery simulation. Our proposed approach (ADMM with CBF) is compared against ADMM without CBFs and the relaxed-barrier penalty method [4]. The disturbance is applied at 0.35 sec.

IV. HARDWARE EXPERIMENTS

This section validates our whole-body NMPC approach on hardware. The hardware results are best captured in the supplementary video accessible on YouTube¹. The NMPC allows the MIT Humanoid to holistically reason about all degrees of freedom while respecting joint limits and self-collision constraints with sufficient accuracy. This enables the robot to coordinate its arm and leg motions to dynamically balance when walking, stopping, and recovering from significant disturbances (Fig. 1). In practice, joint position limits are always respected, allowing the robot to walk stably with its knees fully extended. Combined with the sphere-based collision model from Fig. 2b and CBFs, the robot can reliably plan complex crossed-leg motions that enhance stability in challenging push recovery, abrupt halting, or fast turning scenarios.

As long as they run sufficiently fast, the different NMPC formulations transfer seamlessly to hardware. Table I shows the solve times of four NMPC formulations extensively tested on hardware with 20 ADMM iterations. The full collision model (Fig. 2b) only increases solve times by 9%, and the CBFs only increase solve times by 2.7%. Note that the standard deviations are low due to the fixed number of iterations. The formulation with $dt = 50$ ms is the fastest one that remains stable on hardware and can walk at up to 0.8 m/s at a 200 Hz update rate. The formulation with $dt = 25$ ms is the most successful controller (Fig. 4) that is still fast enough for online only (90 Hz). It can walk at speeds of up to 1.1 m/s on hardware and is much more resistant to push recoveries and rough terrain.

TABLE I: Computation Time Breakdown on the MIT Humanoid’s Computer for 20 ADMM Iterations While Walking

NMPC Formulation		Computation Time (ms)			
dt (ms)	Collision Model	QP Data	QP Step	Line Search	Total mean (std)
50	Simple	0.9	3.3	0.13	4.3 (0.2)
50	Full	1.0	3.5	0.15	4.7 (0.2)
25	Full	2.8	7.8	0.4	11.0 (0.2)
25	Full + CBF	2.9	7.9	0.5	11.3 (0.2)

V. CONCLUSION AND OUTLOOK

This paper presented an implementation of whole-body NMPC that plans trajectories for all the degrees of freedom of the MIT Humanoid in real time. Our simulation results suggest that real robots may not benefit from high-accuracy solutions due to unavoidable inertial modeling errors, dynamics discretization errors and computation delay. Instead of seeking high accuracy, we leverage ADMM’s ability to provide reliable, low-accuracy solutions at a high frequency and show their adequacy through extensive hardware experiments. Furthermore, we use CBFs at the first timestep of the NMPC to enhance the closed-loop feasibility of self-collision constraints with minimal added computational burden. Our approach enables the MIT Humanoid to reliably walk and respond to significant disturbances with holistic whole-body

reasoning while respecting contact constraints, joint limits, and self-collisions. This allows the robot to execute arm and crossed-leg motions that enhance stability.

Despite its empirical reliability, our approach cannot guarantee stability or feasibility of the solution. Additionally, the proposed approach follows a fixed contact sequence, making the controller vulnerable to larger pushes when applied at the beginning of a swing phase. Finally, the most successful controllers in simulation are still too slow for hardware deployment. Our solver can be accelerated by state-of-the-art advancements such as analytical derivatives [9], parallelization [10], and structure-exploiting Riccati factorizations [35].

VI. ACKNOWLEDGMENTS

We thank Andrew SaLoutos, Hongmin Kim and David Nguyen for continuously robustifying the hardware.

REFERENCES

- [1] A. Herdt, H. Diedam, P.-B. Wieber, D. Dimitrov, K. Mombaur, and M. Diehl, “Online Walking Motion Generation with Automatic Footstep Placement,” *Advanced Robotics*, vol. 24, no. 5-6, pp. 719–737, Jan. 2010, ISSN: 0169-1864. DOI: 10.1163/016918610X493552. (visited on 07/04/2022).
- [2] D. Kim, J. Di Carlo, B. Katz, G. Bledt, and S. Kim, “Highly Dynamic Quadruped Locomotion via Whole-Body Impulse Control and Model Predictive Control,” *arXiv:1909.06586 [cs]*, Sep. 2019. arXiv: 1909.06586 [cs]. (visited on 09/01/2020).
- [3] R. Grandia, A. J. Taylor, A. D. Ames, and M. Hutter, “Multi-Layered Safety for Legged Robots via Control Barrier Functions and Model Predictive Control,” in *2021 IEEE International Conference on Robotics and Automation (ICRA)*, May 2021, pp. 8352–8358. DOI: 10.1109/ICRA48506.2021.9561510.
- [4] R. Grandia, F. Jenelten, S. Yang, F. Farshidian, and M. Hutter, “Perceptive Locomotion Through Nonlinear Model-Predictive Control,” *IEEE Transactions on Robotics*, pp. 1–20, 2023, ISSN: 1941-0468. DOI: 10.1109/TRO.2023.3275384.
- [5] C. Khazoom, D. Gonzalez-Diaz, Y. Ding, and S. Kim, *Humanoid Self-Collision Avoidance Using Whole-Body Control with Control Barrier Functions*, Nov. 2022. DOI: 10.48550/arXiv.2207.00692. arXiv: 2207.00692 [cs]. (visited on 01/03/2023).
- [6] J. Nocedal and S. J. Wright, *Numerical Optimization* (Springer Series in Operations Research), 2nd ed. New York: Springer, 2006, ISBN: 978-0-387-30303-1.
- [7] B. D. MAYNE, “A Second-order Gradient Method for Determining Optimal Trajectories of Non-linear Discrete-time Systems,” *International Journal of Control*, vol. 3, no. 1, pp. 85–95, Jan. 1966, ISSN: 0020-7179. DOI: 10.1080/00207176608921369. (visited on 12/27/2020).
- [8] M. Diehl, H. G. Bock, and J. P. Schlöder, “A Real-Time Iteration Scheme for Nonlinear Optimization in Optimal Feedback Control,” *SIAM Journal on Control and Optimization*, vol. 43, no. 5, pp. 1714–1736, Jan. 2005, ISSN: 0363-0129, 1095-7138. DOI: 10.1137/S0363012902400713. (visited on 05/22/2024).
- [9] J. Carpentier and N. Mansard, “Analytical Derivatives of Rigid Body Dynamics Algorithms,” in *Robotics: Science and Systems XIV*, Robotics: Science and Systems Foundation, Jun. 2018, ISBN: 978-0-9923747-4-7. DOI: 10.15607/RSS.2018.XIV.038. (visited on 05/30/2024).
- [10] S. Katayama and T. Ohtsuka, “Efficient solution method based on inverse dynamics for optimal control problems of rigid body systems,” in *2021 IEEE International Conference on Robotics and Automation (ICRA)*, May 2021, pp. 2070–2076. DOI: 10.1109/ICRA48506.2021.9561109. (visited on 10/12/2023).
- [11] S. Katayama, M. Murooka, and Y. Tazaki, “Model predictive control of legged and humanoid robots: Models and algorithms,” *Advanced Robotics*, vol. 37, no. 5, pp. 298–315, Mar. 2023, ISSN: 0169-1864. DOI: 10.1080/01691864.2023.2168134. (visited on 01/29/2024).

¹<https://youtu.be/Xmi7AFGh1Fc>

- [12] W. Jallet, E. Dantec, E. Arlaud, J. Carpentier, and N. Mansard, *Parallel and Proximal Linear-Quadratic Methods for Real-Time Constrained Model-Predictive Control*, May 2024. arXiv: 2405.09197 [cs, math]. (visited on 05/18/2024).
- [13] M. Neunert, M. Stäuble, M. Giffthaler, *et al.*, “Whole-Body Non-linear Model Predictive Control Through Contacts for Quadrupeds,” *IEEE Robotics and Automation Letters*, vol. 3, no. 3, pp. 1458–1465, Jul. 2018, ISSN: 2377-3766. DOI: 10.1109/LRA.2018.2800124.
- [14] J.-P. Sleiman, F. Farshidian, M. V. Minniti, and M. Hutter, “A Unified MPC Framework for Whole-Body Dynamic Locomotion and Manipulation,” *IEEE Robotics and Automation Letters*, vol. 6, no. 3, pp. 4688–4695, Jul. 2021, ISSN: 2377-3766. DOI: 10.1109/LRA.2021.3068908.
- [15] C. Mastalli, S. P. Chhatoi, T. Corbères, S. Tonneau, and S. Vijayakumar, “Inverse-Dynamics MPC via Nullspace Resolution,” *IEEE Transactions on Robotics*, pp. 1–20, 2023, ISSN: 1941-0468. DOI: 10.1109/TRO.2023.3262186.
- [16] J. Koenemann, A. Del Prete, Y. Tassa, *et al.*, “Whole-body model-predictive control applied to the HRP-2 humanoid,” in *2015 IEEE/RSJ International Conference on Intelligent Robots and Systems (IROS)*, Sep. 2015, pp. 3346–3351. DOI: 10.1109/IROS.2015.7353843.
- [17] E. Dantec, M. Naveau, P. Fernbach, *et al.*, “Whole-Body Model Predictive Control for Biped Locomotion on a Torque-Controlled Humanoid Robot,” in *2022 IEEE-RAS 21st International Conference on Humanoid Robots (Humanoids)*, Ginowan, Japan: IEEE, Nov. 2022, pp. 638–644, ISBN: 9798350309799. DOI: 10.1109/Humanoids53995.2022.10000129. (visited on 04/19/2023).
- [18] A. G. Pandala, Y. Ding, and H.-W. Park, “qpSWIFT: A Real-Time Sparse Quadratic Program Solver for Robotic Applications,” *IEEE Robotics and Automation Letters*, vol. 4, no. 4, pp. 3355–3362, Oct. 2019, ISSN: 2377-3766. DOI: 10.1109/LRA.2019.2926664. (visited on 05/28/2024).
- [19] G. Frison and M. Diehl, “HPIPM: A high-performance quadratic programming framework for model predictive control*,” *IFAC-PapersOnLine*, 21st IFAC World Congress, vol. 53, no. 2, pp. 6563–6569, Jan. 2020, ISSN: 2405-8963. DOI: 10.1016/j.ifacol.2020.12.073. (visited on 05/28/2024).
- [20] R. Schwan, Y. Jiang, D. Kuhn, and C. N. Jones, *PIQP: A Proximal Interior-Point Quadratic Programming Solver*, Sep. 2023. DOI: 10.48550/arXiv.2304.00290. arXiv: 2304.00290 [math]. (visited on 05/28/2024).
- [21] Z. Xie, C. K. Liu, and K. Hauser, “Differential dynamic programming with nonlinear constraints,” in *2017 IEEE International Conference on Robotics and Automation (ICRA)*, May 2017, pp. 695–702. DOI: 10.1109/ICRA.2017.7989086. (visited on 05/28/2024).
- [22] A. Bambade, F. Schramm, S. E. Kazdadi, S. Caron, A. Taylor, and J. Carpentier, “PROXQP: An Efficient and Versatile Quadratic Programming Solver for Real-Time Robotics Applications and Beyond,” W. Jallet, A. Bambade, E. Arlaud, S. El-Kazdadi, N. Mansard, and J. Carpentier, “PROXDDP: Proximal Constrained Trajectory Optimization.”
- [23] T. A. Howell, B. E. Jackson, and Z. Manchester, “ALTRO: A Fast Solver for Constrained Trajectory Optimization,” in *2019 IEEE/RSJ International Conference on Intelligent Robots and Systems (IROS)*, Nov. 2019, pp. 7674–7679. DOI: 10.1109/IROS40897.2019.8967788.
- [24] J.-R. Chiu, J.-P. Sleiman, M. Mittal, F. Farshidian, and M. Hutter, “A Collision-Free MPC for Whole-Body Dynamic Locomotion and Manipulation,” in *2022 International Conference on Robotics and Automation (ICRA)*, Philadelphia, PA, USA: IEEE, May 2022, pp. 4686–4693, ISBN: 978-1-72819-681-7. DOI: 10.1109/ICRA46639.2022.9812280. (visited on 05/28/2024).
- [25] J.-P. Sleiman, F. Farshidian, and M. Hutter, “Constraint Handling in Continuous-Time DDP-Based Model Predictive Control,” in *2021 IEEE International Conference on Robotics and Automation (ICRA)*, May 2021, pp. 8209–8215. DOI: 10.1109/ICRA48506.2021.9560795.
- [26] S. Boyd, “Distributed Optimization and Statistical Learning via the Alternating Direction Method of Multipliers,” *Foundations and Trends® in Machine Learning*, vol. 3, no. 1, pp. 1–122, 2010, ISSN: 1935-8237, 1935-8245. DOI: 10.1561/2200000016. (visited on 06/07/2023).
- [27] R. Budhiraja, J. Carpentier, and N. Mansard, “Dynamics Consensus between Centroidal and Whole-Body Models for Locomotion of Legged Robots,” in *2019 International Conference on Robotics and Automation (ICRA)*, May 2019, pp. 6727–6733. DOI: 10.1109/ICRA.2019.8793878.
- [28] A. Meduri, P. Shah, J. Viereck, M. Khadiv, I. Havoutis, and L. Righetti, “BiConMP: A Nonlinear Model Predictive Control Framework for Whole Body Motion Planning,” *IEEE Transactions on Robotics*, vol. 39, no. 2, pp. 905–922, Apr. 2023, ISSN: 1552-3098, 1941-0468. DOI: 10.1109/TRO.2022.3228390. (visited on 05/29/2024).
- [29] G. Bravo-Palacios and P. M. Wensing, “Large-Scale ADMM-based Co-Design of Legged Robots,” in *2022 IEEE/RSJ International Conference on Intelligent Robots and Systems (IROS)*, Oct. 2022, pp. 8842–8849. DOI: 10.1109/IROS47612.2022.9981641.
- [30] A. Aydinoglu and M. Posa, “Real-Time Multi-Contact Model Predictive Control Via ADMM,” p. 8,
- [31] B. Stellato, G. Banjac, P. Goulart, A. Bemporad, and S. Boyd, “OSQP: An operator splitting solver for quadratic programs,” *Mathematical Programming Computation*, vol. 12, no. 4, pp. 637–672, Dec. 2020, ISSN: 1867-2949, 1867-2957. DOI: 10.1007/s12532-020-00179-2. (visited on 06/07/2023).
- [32] J. A. E. Andersson, J. Gillis, G. Horn, J. B. Rawlings, and M. Diehl, “CasADi: A software framework for nonlinear optimization and optimal control,” *Mathematical Programming Computation*, vol. 11, no. 1, pp. 1–36, Mar. 2019, ISSN: 1867-2949, 1867-2957. DOI: 10.1007/s12532-018-0139-4. (visited on 01/05/2021).
- [33] R. Verschuere, G. Frison, D. Kouzoupis, *et al.*, “Acados—a modular open-source framework for fast embedded optimal control,” *Mathematical Programming Computation*, vol. 14, no. 1, pp. 147–183, Mar. 2022, ISSN: 1867-2957. DOI: 10.1007/s12532-021-00208-8. (visited on 05/28/2024).
- [34] A. Jordana, S. Kleff, A. Meduri, J. Carpentier, N. Mansard, and L. Righetti, “Stagewise Implementations of Sequential Quadratic Programming for Model-Predictive Control,”
- [35] G. Bledt and S. Kim, “Implementing Regularized Predictive Control for Simultaneous Real-Time Footstep and Ground Reaction Force Optimization,” in *2019 IEEE/RSJ International Conference on Intelligent Robots and Systems (IROS)*, Nov. 2019, pp. 6316–6323. DOI: 10.1109/IROS40897.2019.8968031.
- [36] Q. Nguyen and K. Sreenath, “Exponential Control Barrier Functions for enforcing high relative-degree safety-critical constraints,” in *2016 American Control Conference (ACC)*, Jul. 2016, pp. 322–328. DOI: 10.1109/ACC.2016.7524935.
- [37] A. D. Ames, S. Coogan, M. Egerstedt, G. Notomista, K. Sreenath, and P. Tabuada, “Control Barrier Functions: Theory and Applications,” in *2019 18th European Control Conference (ECC)*, Jun. 2019, pp. 3420–3431. DOI: 10.23919/ECC.2019.8796030.
- [38] A. SaLoutos, E. Stanger-Jones, Y. Ding, M. Chignoli, and S. Kim, “Design and Development of the MIT Humanoid: A Dynamic and Robust Research Platform,” in *2023 IEEE-RAS 22nd International Conference on Humanoid Robots (Humanoids)*, Dec. 2023, pp. 1–8. DOI: 10.1109/Humanoids57100.2023.10375199. (visited on 06/09/2024).
- [39] A. Jain, “Recursive Algorithms Using Local Constraint Embedding for Multibody System Dynamics.” DOI: 10.1115/DETC2009-87663. (visited on 06/28/2024).
- [40] M. Chignoli, N. Adrian, S. Kim, and P. M. Wensing, *Recursive Rigid-Body Dynamics Algorithms for Systems with Kinematic Loops*, Nov. 2023. DOI: 10.48550/arXiv.2311.13732. arXiv: 2311.13732 [cs]. (visited on 05/21/2024).
- [41] A. Reuther, J. Kepner, C. Byun, *et al.*, “Interactive Supercomputing on 40,000 Cores for Machine Learning and Data Analysis,” in *2018 IEEE High Performance Extreme Computing Conference (HPEC)*, Sep. 2018, pp. 1–6. DOI: 10.1109/HPEC.2018.8547629. (visited on 05/30/2024).
- [42] A. Wang and S. Kim, “Directional efficiency in geared transmissions: Characterization of backdrivability towards improved proprioceptive control,” in *2015 IEEE International Conference on Robotics and Automation (ICRA)*, May 2015, pp. 1055–1062. DOI: 10.1109/ICRA.2015.7139307. (visited on 06/29/2024).